Ultrasonics Sonochemistry 94 (2023) 106352

Contents lists available at ScienceDirect

Ultrasonics Sonochemistry

journal homepage: www.elsevier.com/locate/ultson

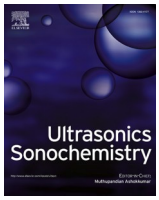

Translation of cavitation bubble near the different walls

Shaoyang Kou, Weizhong Chen *, Yaorong Wu, Guoying Zhao

Key Laboratory of Modern Acoustics, Ministry of Education, Institution of Acoustics, Nanjing University, Nanjing 210093, China

ARTICLE INFO

Keywords:
Cavitation bubble
Walls
Method of images
Two bubble dynamics

ABSTRACT

The interaction between spherical cavitation bubble and flat wall is transformed into that between the real bubble and imaging bubble by the method of images. Firstly, we investigate the dynamics of real bubble and matched, inversed or mis-matched imaging bubble driven by a small amplitude ultrasound, revealing the characteristics of the interaction between cavitation bubble and rigid, soft and impedance walls. Then, we emphatically study the dynamics of real bubble and mis-matched imaging bubble driven by a finite amplitude ultrasound, and the interaction characteristics between cavitation bubble and real impedance wall are revealed. The results show that the cavitation bubble is always close to the rigid wall and far away from the soft wall; For the impedance wall, whether the cavitation bubble is far away or close depends on the specific wall parameters. Moreover, the direction and magnitude of bubble's translation velocity can be changed by adjusting the driving parameters. Understanding the interaction between cavitation bubble and impedance wall is of great significance for efficient application of ultrasonic cavitation.

1. Introduction

The propagation of ultrasonic waves in the liquid causes the changes of pressure, which lead to the growth of structural defects (cavitation nuclei) in the liquid into visible bubbles. This phenomenon is called ultrasonic cavitation and the bubbles are named as the cavitation bubbles [1–3]. Under the action of ultrasonic waves, cavitation bubbles will have radial pulsations. The dynamic model of a single cavitation bubble originated from Rayleigh's pioneering work [4], and supplemented by Plesset *et al.* [5], relatively complete single bubble dynamic theories have been formed [6]. On this basis, people put forward the two-bubble dynamic model [7]. In 2001, Doinikov applied the fluid dynamics in the framework of Lagrangian mechanism to propose a movable two-bubble dynamic model [8]. Zhang *et al.* also constructed the motion equations of two-bubble by directly integrating the surface pressure of bubble in the framework of Newtonian mechanism [9]. Through the two-bubble dynamic model, people can understand the interaction between cavitation bubbles [10–12], and the properties [13–16] of the second Bjerknes force [17]. People have proposed many dynamic models [18,19] and well explained bubble dynamics in the free space. In 1971, Plesset studied a single bubble near a rigid wall and showed an apple-shape distorted bubble [20] which agreed with the experimental [21]. Due to the analytical solution difficulty of point source near the flat wall, people can only use computers for numerical solution. With the method of images [22] and the two-bubble dynamic model [7,8], the rigid wall problem of cavitation bubble was solved [23–26]. The method of images first appeared in electrodynamics [22]. The induced charges on the conductor surface is replaced by the imaging charge in the extended space to solve the problem of charge near wall, thus the analytical solution difficulty of spherical point charge near the flat wall was solved.

Of course, the rigid wall is only an ideal case among a great variety of real walls, which is only applicable to the wall that is much harder than the host liquid. In addition to the rigid wall, there are also ideal soft wall and real impedance wall in between. In this paper, the method of images is extended to all walls, including soft and impedance walls. By solving the two-bubble dynamics of real bubble and imaging bubble, the complete wall behavior of cavitation bubble is obtained.

2. Wall properties and imaging bubble

2.1. The behaviors of ultrasonic waves at walls

Wall behavior occurs when a plane ultrasonic wave with the vibration velocity of v_i and the acoustic pressure of p_i passes from one medium to another. According to the acoustic properties at the interface of two media, the walls can be divided into three types: rigid wall, soft wall and impedance wall in between. The characteristics of ultrasonic wave and conditions of velocity potential at these walls are shown in Table 1,

* Corresponding author.
E-mail address: wzchen@nju.edu.cn (W. Chen).

https://doi.org/10.1016/j.ultsonch.2023.106352
Received 9 January 2023; Received in revised form 15 February 2023; Accepted 27 February 2023
Available online 3 March 2023

Table 1
Characteristics of ultrasonic wave and conditions of velocity potential at different walls.

Wall types	Wall conditions	Imaging bubble
Rigid wall	$v\|_S = 0$	Matched imaging bubble
Soft wall	$p\|_S = 0$	Inversed imaging bubble
Impedance wall	$v\|_S > 0, p\|_S > 0$	Mis-matched imaging bubble

where α and β are constants, $v|_S$, $p|_S$ denote the vibration velocity and acoustic pressure of the fluid at the center line (surface) between two bubbles.

2.2. Imaging bubble

We consider a spherical cavitation bubble B located near the wall S in the liquid with the density ρ, sound speed c, the viscosity η and surface tension σ driven by the ultrasound $P_d(t)$ (see Fig. 1). Since cavitation bubbles are usually very small, the wall can be regarded as flat, which makes the analytical solution of the problem difficult. Inspired by the method of images in electrodynamics [22], we now extend the real half space to full space composed of real space and imaging space (shadow region in Fig. 1), and place an imaging bubble B′ in the imaging space driven by the ultrasound $P_d'(t)$. In this way, the problem of single bubble near the wall in half space is transformed into two-bubble problem without the wall in full space which can be solved analytically with the help of the two-bubble dynamic model [8,9].

If the pulsations of real bubble and imaging bubble are matched, that is, the two bubbles have the exactly same pulsations, now the $v|_S$ equals 0, fitting the rigid wall condition (see Table 1); If the pulsations of real bubble and imaging bubble are inversed each other, that is, when the real bubble expands (shrinks), the imaging bubble will shrink (expand) with the same amplitude, so that the $p|_S$ equals 0, fitting the soft wall condition (see Table 1); If the pulsations of real bubble and imaging bubble are mis-matched, that is, when the real bubble expands (shrinks), the imaging bubble will either shrink or expand, and the amplitude may be different. As a result, the $v|_S$ and $p|_S$ are greater than 0, fitting the impedance wall condition (see Table 1). The last column of Table 1 shows the pulsating phase of imaging bubble relative to real bubble corresponding to different walls.

3. Dynamics model of real bubble and imaging bubble

3.1. Doinikov two-bubble dynamic model

We introduce the ground coordinate system $O-x$, see Fig. 1. The real bubble and imaging bubble are respectively located at $X(t)$ and $X'(t)$ at time t, with the center spacing of $D(t) = X(t) - X'(t)$. $R(t)$ and $R'(t)$ denote the radius of real bubble and imaging bubble respectively. At the initial time, their corresponding values are X_0, X_0', D_0, R_0 and R_0', respectively. In the theoretical framework of Doinikov two-bubble dynamics [8], taking R, R', X and X' as the generalized coordinates, we can calculate kinetic energy T and potential energy V of the system through the scattered potential φ of real and imaging bubbles, and construct the Lagrangian function $L = T - V$. Finally, four combined ordinary differential equations of second order are obtained just as those in refs. [8,9].

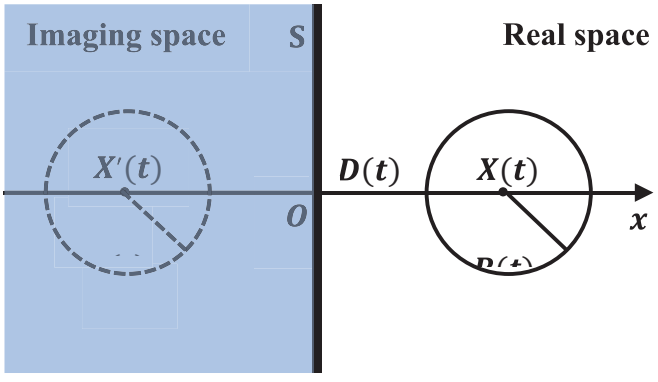

Fig. 1. Diagram for method of images.

According to the method of images, we set the equilibrium radius of imaging bubble the same as real bubble, that is, $R_0 = R_0'$. Moreover, the two bubbles are symmetrically located on both sides of the wall, so the wall's position can be denoted as $X_S = [X(t) + X'(t)]/2$. At the initial time $X_0 = -X_0'$, the wall is at the origin. The wall will usually move due to the movements of the bubbles.

Unfortunately, the real bubble and imaging bubble cannot realize inversed pulsations because the radial pulsations of bubbles are nonlinear. However, they can pulsate inversely each other if they are driven by a small amplitude ultrasound.

3.2. The small amplitude approximation

Considering that the shrink and expansion of bubble become symmetrical when the bubble is driven slightly, then the radial pulsations of real bubble and imaging bubble can be inversed each other. We use perturbation method to expand Doinikov's two-bubble motion equations [8] now, to make the pulsations linear.

When the driving ultrasounds P_d and P_d' are small, bubbles will make slight pulsations, which lead to slighter bubbles' translations. Therefore, we can handle by the following order of magnitude:

$$\begin{aligned} P_d &= \varepsilon p_d, \\ P_d' &= \varepsilon p_d', \\ R &= R_0 + \varepsilon r, \\ R' &= R_0' + \varepsilon r', \\ X &= X_0 + \varepsilon^2 x, \\ X' &= X_0' + \varepsilon^2 x', \\ D &= D_0 + \varepsilon^2 d, \end{aligned} \tag{1}$$

where ε is a small dimensionless parameter, and the physical quantities in lowercase represent the time-dependent parts of the corresponding capital quantities.

Substituting the perturbation expansion (1) into Doinikov's equations [8]:

$$\left(1-\frac{\dot{R}}{c}\right)R\ddot{R} + \left(\frac{3}{2}-\frac{\dot{R}}{2c}\right)\dot{R}^2 - \frac{1}{\rho}\left(1+\frac{\dot{R}}{c}\right)P - \frac{R}{\rho c}\frac{\mathrm{d}P}{\mathrm{d}t} = \frac{\dot{X}}{4} - \frac{R'^2\ddot{R}' + 2R'\dot{R}'^2}{D} + \frac{R'^2\left(\dot{X}\dot{R}' + R'\ddot{X}' + 5\dot{R}'\dot{X}'\right)}{2D^2} - \frac{R'^3\dot{X}'\left(\dot{X} + 2\dot{X}'\right)}{2D^3}, \tag{2}$$

$$\left(1-\frac{\dot{R}'}{c}\right)R'\ddot{R}' + \left(\frac{3}{2}-\frac{\dot{R}'}{2c}\right)\dot{R}'^2 - \frac{1}{\rho}\left(1+\frac{\dot{R}'}{c}\right)P' - \frac{R'}{\rho c}\frac{\mathrm{d}P'}{\mathrm{d}t} = \frac{\dot{X}'}{4} - \frac{R^2\ddot{R} + 2R\dot{R}^2}{D} - \frac{R^2\left(\dot{X}'\dot{R} + R\ddot{X} + 5\dot{R}\dot{X}\right)}{2D^2} - \frac{R^3\dot{X}\left(\dot{X}' + 2\dot{X}\right)}{2D^3}, \tag{3}$$

$$\frac{R\ddot{X}}{3} + \dot{R}\dot{X} + \frac{1}{D^2}\frac{\mathrm{d}}{\mathrm{d}t}\left(RR'^2\dot{R}'\right) - \frac{R'^2\left(RR'\ddot{X}' + R'\dot{R}\dot{X}' + 5R\dot{R}'\dot{X}'\right)}{D^3} = \frac{F_{ex}}{2\pi\rho R^2}, \tag{4}$$

$$\frac{R'\ddot{X}'}{3} + \dot{R}'\dot{X}' - \frac{1}{D^2}\frac{\mathrm{d}}{\mathrm{d}t}\left(R'R^2\dot{R}\right) - \frac{R^2\left(RR'\ddot{X} + R\dot{R}'\dot{X} + 5R\dot{R}\dot{X}\right)}{D^3} = \frac{F_{ex}'}{2\pi\rho R'^2}, \tag{5}$$

where P and $P^{'}$ can be represented as:

$$P = \left(P_0 + \frac{2\sigma}{R_0}\right)\left(\frac{R_0}{R}\right)^{3\gamma} - \frac{2\sigma}{R} - \frac{4\eta\dot{R}}{R} - P_0 - P_{\mathrm{d}}(t), \tag{6}$$

$$P^{'} = \left(P_0 + \frac{2\sigma}{R_0^{'}}\right)\left(\frac{R_0^{'}}{R^{'}}\right)^{3\gamma} - \frac{2\sigma}{R^{'}} - \frac{4\eta\dot{R}^{'}}{R^{'}} - P_0 - P_{\mathrm{d}}^{'}(t), \tag{7}$$

the external forces F_{ex} and $F_{\mathrm{ex}}^{'}$ are set to be:

$$F_{\mathrm{ex}} = -12\pi\eta R\left(\dot{X} - v^{'}\right), \tag{8}$$

$$F_{\mathrm{ex}}^{'} = -12\pi\eta R^{'}\left(\dot{X}^{'} - v\right), \tag{9}$$

where v ($v^{'}$) denotes the velocity of liquid which is generated by real (imaging) bubble at the center of imaging (real) bubble:

$$v = -\frac{-R^2\dot{R}}{D^2} + \frac{R^3\dot{X}}{D^3}, \tag{10}$$

$$v^{'} = -\frac{R^{'2}\dot{R}^{'}}{D^2} + \frac{R^{'3}\dot{X}^{'}}{D^3}. \tag{11}$$

Merging the results according to the powers of ε, and letting the coefficients of each power of ε to be zero respectively, we can obtain:

$\boldsymbol{\varepsilon}^0$ coefficient equations:

$$-\frac{1}{\rho}\left(P_0 + \frac{2\sigma}{R_0}\right) + \frac{2\sigma}{\rho R_0} + \frac{P_0}{\rho} = 0, \tag{12}$$

$$-\frac{1}{\rho}\left(P_0 + \frac{2\sigma}{R_0^{'}}\right) + \frac{2\sigma}{\rho R_0^{'}} + \frac{P_0}{\rho} = 0, \tag{13}$$

$\boldsymbol{\varepsilon}^1$ coefficient equations:

$$\begin{aligned}&\left(R_0 + \frac{4\eta}{\rho c}\right)\ddot{r} + \left[\frac{1}{\rho c}(3\gamma - 1)\left(P_0 + \frac{2\sigma}{R_0}\right) + \frac{P_0}{\rho c} + \frac{4\eta}{\rho R_0}\right]\dot{r} - \frac{p_{\mathrm{d}}}{\rho} - \frac{R_0\dot{p}_{\mathrm{d}}}{\rho c} + \left[\frac{3\gamma}{\rho R_0}\left(P_0 + \frac{2\sigma}{R_0}\right) - \frac{2\sigma}{\rho R_0^2}\right]r \\ &= -\frac{R_0^{'2}}{D_0}\ddot{r}^{'},\end{aligned} \tag{14}$$

$$\begin{aligned}&\left(R_0^{'} + \frac{4\eta}{\rho c}\right)\ddot{r}^{'} + \left[\frac{1}{\rho c}(3\gamma - 1)\left(P_0 + \frac{2\sigma}{R_0^{'}}\right) + \frac{P_0}{\rho c} + \frac{4\eta}{\rho R_0^{'}}\right]\dot{r}^{'} - \frac{p_{\mathrm{d}}^{'}}{\rho} - \frac{R_0^{'}\dot{p}_{\mathrm{d}}^{'}}{\rho c} + \left[\frac{3\gamma}{\rho R_0^{'}}\left(P_0 + \frac{2\sigma}{R_0^{'}}\right) - \frac{2\sigma}{\rho R_0^{'2}}\right]r^{'} \\ &= -\frac{R_0^2}{D_0}\ddot{r},\end{aligned} \tag{15}$$

$\boldsymbol{\varepsilon}^2$ coefficient equations:

$$\begin{aligned}&\frac{R_0^2}{3}\ddot{x} - \frac{R_0R_0^{'}\dot{r}^{'}\left(R_0^{'}\dot{r} + 2R_0\dot{r}^{'}\right)}{D_0^2} - \frac{2R_0R_0^{'}\left(R_0^{'}r + R_0r^{'}\right)}{D_0^2}\ddot{r}^{'} - \frac{R_0^{'3}R_0^2}{D_0^3}\ddot{x}^{'} \\ &= -\frac{6\eta}{\rho}\left(\dot{x} - \frac{2R_0^{'}r^{'}\dot{r}^{'}}{D_0^2} - \frac{R_0^{'3}\dot{x}^{'}}{D_0^3}\right),\end{aligned} \tag{16}$$

$$\begin{aligned}&\frac{R_0^{'2}}{3}\ddot{x}^{'} + \frac{R_0^{'}R_0\dot{r}\left(R_0\dot{r}^{'} + 2R_0^{'}\dot{r}\right)}{D_0^2} + \frac{2R_0^{'}R_0\left(R_0r^{'} + R_0^{'}r\right)}{D_0^2}\ddot{r} - \frac{R_0^3R_0^{'2}}{D_0^3}\ddot{x} \\ &= -\frac{6\eta}{\rho}\left(\dot{x}^{'} + \frac{2R_0r\dot{r}}{D_0^2} - \frac{R_0^3\dot{x}}{D_0^3}\right),\end{aligned} \tag{17}$$

where P_0 is the hydrostatic pressure, γ is the polytropic exponent of the gas within the bubble, and ω is the angular frequency. We choose the driving ultrasounds as $P_{\mathrm{d}}(t) = -P_{\mathrm{a}}\sin\omega t$ and $P_{\mathrm{d}}^{'}(t) = -P_{\mathrm{a}}\sin(\omega t + \Phi)$ respectively.

Equations (12) and (13) are self-consistent and trivial; Equations (14) and (15) govern the radial pulsations of bubbles, and they are linear equations; Equations (16) and (17) describe the translations of bubbles. Equations (14) - (17) are the leading order approximation of Doinikov's equations [8] driven by a small amplitude ultrasound. It can be seen from Eqs. (14) - (17) that ultrasound drives bubble's pulsation, and bubble's pulsation leads to bubble's translation. The driving ultrasound does not directly lead to bubble's translation, and the bubble's translation does not react on bubble's pulsation. This allows us to obtain the imaging bubble whose pulsation is matched, inversed or mis-matched with the real bubble by adjusting the driving parameters.

4. The translation of bubble near different walls

4.1. The translation of bubble driven by a small amplitude ultrasound

By numerically solving the two-bubble pulsation Equations (14) and (15) driven by a small amplitude ultrasound, we can get the linear radii evolution curves of bubbles, as shown in Fig. 2. Continuing to solve the translation Equations (16) and (17) to obtain the translation evolution curves of bubbles near the rigid, soft and impedance walls (see Fig. 3). The computation parameters are set to $P_0 = 1.013\mathrm{bar}$, $\rho = 998\mathrm{kg/m^3}$, $\sigma = 0.0725\mathrm{N/m}$, $\eta = 0.001\mathrm{Pa{\cdot}s}$, $c = 1500\mathrm{m/s}$, $\gamma = 1.4$, $R_0 = R_0^{'} = 4.5\mu\mathrm{m}$, $D_0 = 200\mu\mathrm{m}$, driving pressure $P_{\mathrm{a}} = 0.4\mathrm{bar}$, and driving frequency $f = 25\mathrm{kHz}$.

In Fig. 3, the interaction between the real and imaging bubbles can be inversely transformed into that between real bubble and walls. As a result, the bubble is close to the rigid wall (solid line) and far away from the soft wall (dashed line). The bubble is close to the impedance wall 1 (dotted line), while, it is far away from the impedance wall 2 (dash-dotted line). Therefore, the impedance wall can show the characteristics of either rigid wall or soft wall according to the difference of wall parameters.

After imaging transformation, the pulsating phase Φ of the imaging bubble relative to the real bubble reflects the acoustic characteristics of

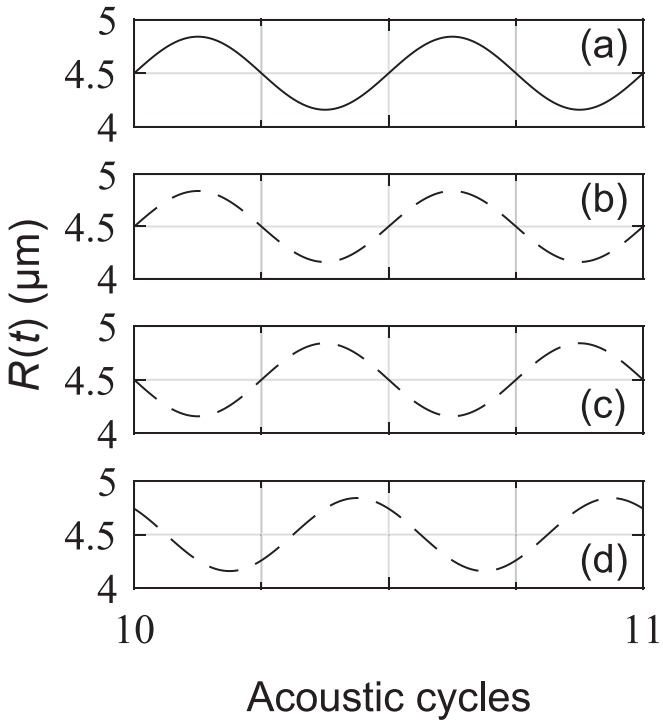

Fig. 2. Pulsation evolution curves of bubbles. (a) Real bubble; (b) Matched imaging bubble; (c) Inversed imaging bubble; (d) Mis-matched imaging bubble ($\Phi = 3\pi/4$).

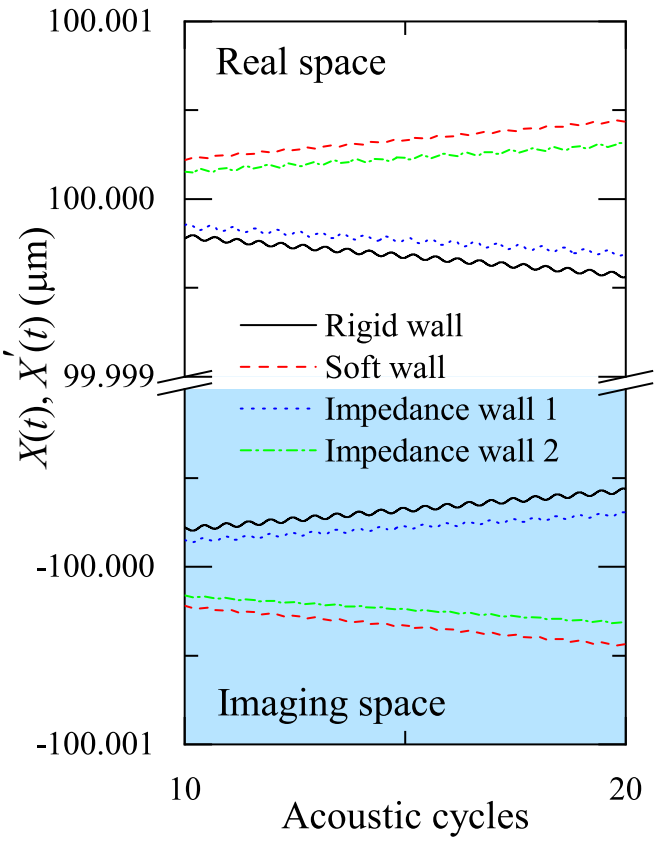

Fig. 3. Translation evolution curves of bubbles. The upper curves correspond to real bubble, and the lower curves correspond to imaging bubble. The phase difference corresponding to the impedance wall 1 and 2 is $\pi/4$ and $3\pi/4$ respectively.

the wall in liquid, and determines the direction and magnitude of bubble's translation velocity relative to the wall. Fig. 4 shows the curve of the periodic averaged translation velocity of bubble relative to the wall

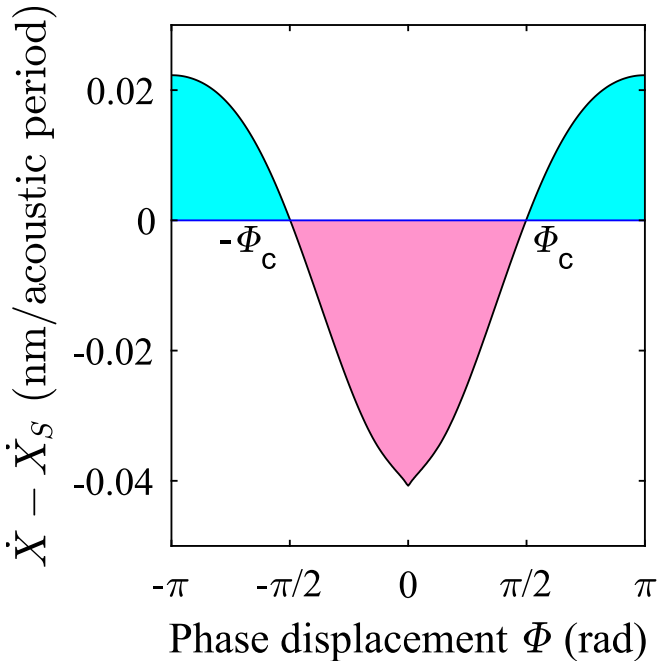

Fig. 4. The curve of bubble's averaged translation velocity as a function of Φ driven by a small amplitude ultrasound.

as a function of Φ. The positive or negative velocity respectively indicates that the bubble is far away from or close to the wall, and the larger its magnitude is, the faster the bubble translates. There is a critical point labelled as Φ_c in Fig. 4. When Φ reaches Φ_c, the bubble dances around some position without translation. When Φ is from 0 to Φ_c, the bubble is close to the wall, and the smaller Φ is, the faster the bubble translates toward the wall; As Φ continues to increase from Φ_c to π, the translation direction of bubble reverses and becomes far away from the wall, and the velocity magnitude of bubble away from the wall gradually increases and reaches the maximum at π. The pink shadow in the figure indicates that the bubble is close to the wall, which is called "matched-like" region; The cyan shadows indicate that the bubble is far away from the wall, which are called "inversed-like" regions.

Through the foregoing, as the wall gradually changes from rigid to soft, the interaction between cavitation bubble and wall gradually decreases from the maximum attraction to 0, and then becomes repulsion force, which reaches the maximum when the wall is soft. And it is a monotonic change.

4.2. *The translation of bubble driven by a finite amplitude ultrasound*

Although the pulsations of bubbles driven by a finite amplitude ultrasound are nonlinear (see Fig. 5), which makes it impossible for the pulsations of real bubble and imaging bubble to reach inversed, we can still obtain the imaging bubbles whose pulsations are matched (see Fig. 5 (b)) and mis-matched (see Fig. 5 (c)) with the real bubble (see Fig. 5 (a)) by solving the Equations (2) - (5). We set to $P_a = 1.1$bar, and the other parameters are the same as those in the subsection 4.1.

Fig. 6 shows the evolution curves of bubbles' translations near the rigid and impedance walls. It can be seen that the bubble is still close to the rigid wall; For the impedance wall, whether the bubble is close or far away depends on the parameters of the wall.

Fig. 7 shows the curve of the periodic averaged translation velocity of bubble relative to the wall as a function of Φ under the driving of a finite amplitude ultrasound. Similarly, the pink shadows in the figure are the

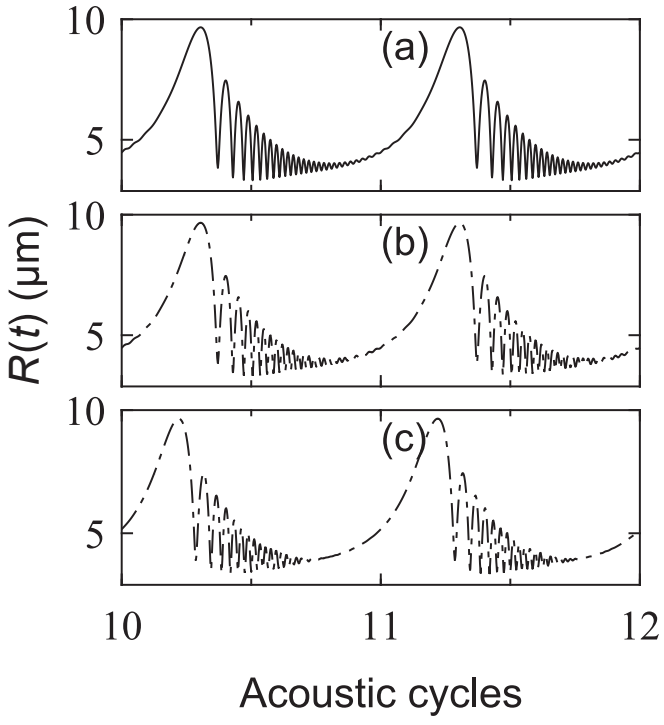

Fig. 5. Pulsation evolution curves of bubbles driven by a finite amplitude ultrasound. (a) Real bubble; (b) Matched imaging bubble; (c) Mis-matched imaging bubble ($\Phi = \pi/6$).

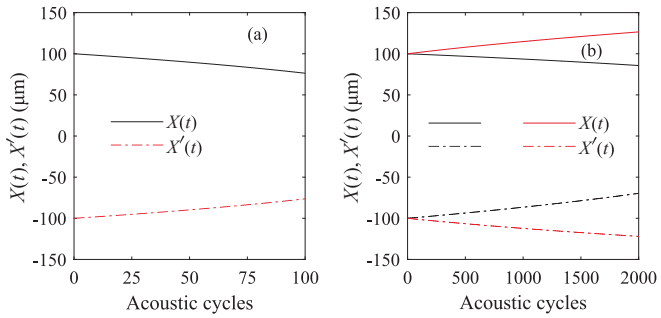

Fig.6. Translation evolution curves of bubbles. (a) Bubbles near rigid wall; (b) Bubbles near impedance wall 3 (black lines) and bubbles near impedance wall 4 (red lines). The phase difference corresponding to the impedance wall 3 and 4 is $\pi/8$ and $\pi/6$ respectively. (For interpretation of the references to colour in this figure legend, the reader is referred to the web version of this article.)

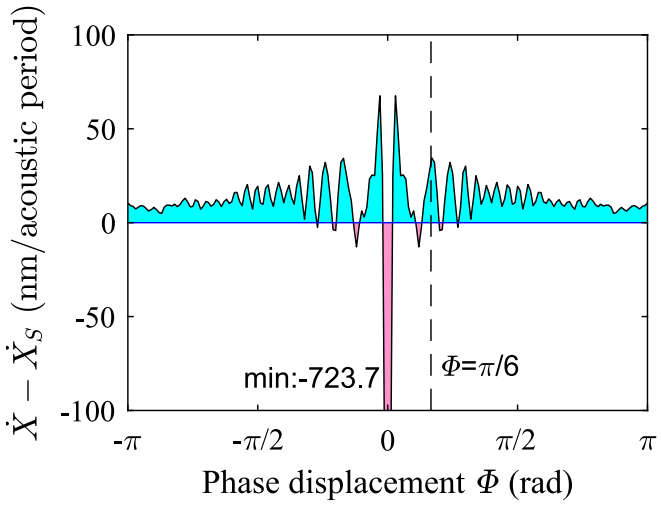

Fig. 7. The curve of bubble's averaged velocity as a function of Φ driven by a finite amplitude ultrasound. The driving parameters are $P_a = 1.1$bar and $f = 25$kHz.

"matched-like" regions, indicating that the bubble is close to the wall, while, the cyan shadows are the "inversed-like" regions, indicating that the bubble is far away from the wall. In Fig. 7 the curve is cut at many points like Φ_c in Fig. 4 by the horizontal axis. As a result, there are several "matched-like" regions in addition to the largest "matched-like" region near $\Phi = 0$ in Fig. 7. This phenomenon is caused by the nonlinear characteristics of bubble pulsation driven by a finite amplitude ultrasound. It can be seen from Fig. 5 (a) that there are many rebound peaks which can be named as the first peak, second peak, third peak and so on in the bubble pulsation curve. When the first peak of real bubble meets the first one of imaging bubble (i.e. matched), the averaged velocity contributes the largest "matched-like" region in Fig. 7. If the first peak of one bubble is aligned with the second or third peak etc. of another bubble, it dedicates the other smaller "matched-like" regions. This phenomenon indicates that the behavior of bubble translating toward or away from the impedance wall alternates repeatedly as the wall material changes. The multi-peak phenomenon of bubble pulsation curve is caused by the nonlinear dynamics driven by a finite amplitude ultrasound. Therefore, this is a nonlinear effect.

To sum up, unlike the monotonic change from the maximum attractive force when the wall is rigid to the maximum repulsive force when the wall is soft driven by a small amplitude ultrasound. Under the driving of a finite amplitude ultrasound, even if one wall repels the cavitation bubble, another wall which is softer than it may attract the cavitation bubble; Although the rigid wall still corresponds to the maximum attraction, but the soft wall does not correspond to the maximum repulsive force anymore, and it is no longer a monotonic change.

4.3. Parametric dependence of bubble's translation

In this section, we will discuss the influence of driving parameters on the translation of bubble near the wall. We set to $D_0 = 200\mu$m, $f = 80$kHz, and the other parameters are the same as those in the subsection 4.1. The curve of the periodic averaged translation velocity of bubble relative to the wall as a function of Φ is obtained, see Fig. 8.

In Fig. 8, it can be found that the two second largest "matched-like" regions are remarkable different from that in Fig. 7. They are not only enlarged in the ratio to the largest "matched-like" region, but also moved in the positions of the critical points. For some phases, such as $\Phi = \pi/6$, the bubble is far away from the wall in Fig. 7, but close to the wall in Fig. 8. Even at the phases close to $\pm\pi$, we can still observe the "matched-like" regions, indicating that cavitation bubble can still translate toward some very soft walls. Furthermore, even in "inversed-like" regions the magnitude of the escaping velocity is also non-monotonic change with the phase. Therefore we can by no means deduce that the softer the wall is, the stronger the repulsive force is. This phenomenon is important for the practical applications of ultrasonic cavitation, such as the ultrasonic cleaning, and makes the ultrasonic cleaning on some relatively soft objects possible.

All these phenomena indicate that we can change the nonlinear characteristics of cavitation bubble's pulsation by changing the driving parameters, so as to change the direction and magnitude of cavitation bubble's translation velocity.

5. Conclusion and discussion

In this paper, the interaction between spherical cavitation bubble and flat wall is transformed into that between two bubbles by the method of images. Firstly, under the driving of a small amplitude ultrasound, bubble pulsation equation is linear while its translation equation is nonlinear. Bubble's pulsation is driven by the ultrasound and leads to its translation. The driving ultrasound does not directly lead to bubble's translation, and the bubble's translation does not react on bubble's pulsation. In addition, The curve of bubble's averaged velocity as a function of Φ is a monotonic change from 0 to π. Secondly, under the driving of a finite amplitude ultrasound, there are many rebound peaks in the bubble pulsation curve, and it is nonlinear. The curve of bubble's averaged velocity as a function of Φ is no longer a monotonic change.

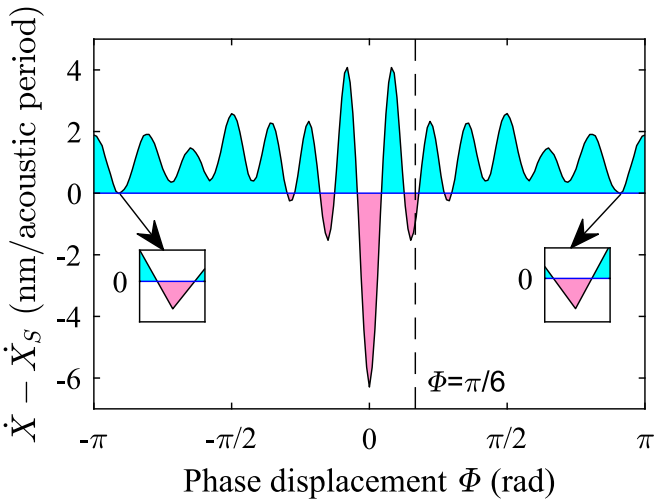

Fig. 8. The curve of bubble's averaged velocity as a function of Φ. The driving parameters are $P_a = 0.85$bar and $f = 80$kHz.

Finally, The influence of driving parameters on the translation of cavitation bubble relative to the wall is also discussed. The results show that the cavitation bubble is always close to the rigid wall and far away from the soft wall; For the impedance wall, whether the cavitation bubble is far away or close depends on the specific wall parameters. Moreover, the direction and magnitude of cavitation bubble's translation velocity can be changed by adjusting the driving parameters. These results are significant on how to make more effective applications of ultrasonic cavitation in the fields of ultrasonic cleaning, ultrasonic extraction, ultrasonic drug delivery and so on. As a preliminary discussion, we have only qualitatively analyzed the corresponding relationship between the pulsating phase Φ of imaging bubble relative to real bubble and the acoustic characteristics of walls at present, and the quantitative relationship between them still needs further investigations.

CRediT authorship contribution statement

Shaoyang Kou: Conceptualization, Methodology, Software, Data curation, Writing – original draft. **Weizhong Chen:** Methodology, Funding acquisition, Supervision. **Yaorong Wu:** Writing – review & editing. **Guoying Zhao:** Writing – review & editing.

Declaration of Competing Interest

The authors declare that they have no known competing financial interests or personal relationships that could have appeared to influence the work reported in this paper.

Acknowledgments

This work was supported by the National Natural Science Foundation of China (Grant No. 12074185).

References

[1] T.G. Leighton, in: The Acoustic Bubble, Academic Press, 1997, https://doi.org/10.1016/B978-0-12-441920-9.X5001-9.
[2] W. Lauterborn, C.D. Ohl, Cavitation bubble dynamics, Ultrason. Sonochem. 4 (1997) 65–75, https://doi.org/10.1016/s1350-4177(97)00009-6.
[3] Y. Shen, W. Chen, L. Zhang, Y. Wu, S. Kou, G. Zhao, The dynamics of cavitation bubbles in a sealed vessel, Ultrason. Sonochem. 82 (2022), 105865, https://doi.org/10.1016/j.ultsonch.2021.105865.
[4] L. Rayleigh, On the pressure developed in a liquid during the collapse of a spherical cavity, Phil. Mag. 34 (1917) 94–98, https://doi.org/10.1080/14786440808635681.
[5] M.S. Plesset, The dynamics of cavitation bubbles, J. Appl. Mech.-Trans. ASME 16 (1949) 277–282, https://doi.org/10.1007/BF02120348.
[6] A.V. Pandit, V.P. Sarvothaman, V.V. Ranade, Estimation of chemical and physical effects of cavitation by analysis of cavitating single bubble dynamics, Ultrason. Sonochem. 77 (2021) 105677.
[7] A. Shima, Natural frequencies of 2 spherical bubbles oscillating in water, J. Basic Eng. 93 (1971) 426-&, https://doi.org/10.1115/1.3425268.
[8] A.A. Doinikov, Translational motion of two interacting bubbles in a strong acoustic field, Phys. Rev. E 64 (2001), 026301, https://doi.org/10.1103/PhysRevE.64.026301.
[9] L. Zhang, W. Chen, Y. Zhang, Y. Wu, X. Wang, G. Zhao, Bubble translation driven by pulsation in a double-bubble system, Chin. Phys. B 29 (03) (2020), 034303, https://doi.org/10.1088/1674-1056/ab69ee.
[10] Y. Shen, L. Zhang, Y. Wu, W. Chen, The role of the bubble?bubble interaction on radial pulsations of bubbles, Ultrason. Sonochem. 73 (2021), 105535, https://doi.org/10.1016/j.ultsonch.2021.105535.
[11] D. Qin, Q. Zou, S. Lei, W. Wang, Z. Li, Nonlinear dynamics and acoustic emissions of interacting cavitation bubbles in viscoelastic tissues, Ultrason. Sonochem. 78 (2021), 105712, https://doi.org/10.1016/j.ultsonch.2021.105712.
[12] Y. Ma, G. Zhang, T. Ma, Interaction of two bubbles with distortion in an acoustic field, Ultrason. Sonochem. 84 (2022), 105953, https://doi.org/10.1016/j.ultsonch.2022.105953.
[13] Y. Zhang, Y. Zhang, S. Li, The secondary Bjerknes force between two gas bubbles under dual-frequency acoustic excitation, Ultrason. Sonochem. 29 (2016) 129–145, https://doi.org/10.1016/j.ultsonch.2015.08.022.
[14] H. Chen, Z. Lai, Z. Chen, Y. Li, The secondary Bjerknes force between two oscillating bubbles in Kelvin-Voigt-type viscoelastic fluids driven by harmonic ultrasonic pressure, Ultrason. Sonochem. 52 (2019) 344–352, https://doi.org/10.1016/j.ultsonch.2018.12.007.
[15] L. Zhang, W. Chen, Y. Wu, Y. Shen, G. Zhao, Repulsive bubble-bubble interaction in ultrasonic field, Chin. Phys. B 30 (10) (2021), 104301, https://doi.org/10.1088/1674-1056/abea98.
[16] X. Zhang, F. Li, C. Wang, R. Mo, J. Hu, J. Guo, S. Lin, Effects of translational motion on the Bjerknes forces of bubbles activated by strong acoustic waves, Ultrasonics 126 (2022), 106809, https://doi.org/10.1016/j.ultras.2022.106809.
[17] V. Bjerknes, Fields of force, Columbia University Press, 1906 https://doi.org/lccn.loc.gov/a11000439.
[18] L. Trilling, The collapse and rebound of a gas bubble, J. Appl. Phys. 23 (1952) 14–17, https://doi.org/10.1063/1.1701962.
[19] J.B. Keller, M. Miksis, Bubble oscillations of large-amplitude, J. Acoust. Soc. Am. 68 (1980) 628–633, https://doi.org/10.1121/1.384720.
[20] M.S. Plesset, R.B. Chapman, Collapse of an initially spherical vapour cavity in neighbourhood of a solid boundary, J. Fluid Mech., 47 (1971) 283-&, https://doi.org/10.1017/s0022112071001058.
[21] W. Lauterborn, H. Bolle, Experimental investigation of cavitation-bubble collapse in neighbourhood of a solid boundary, J. Fluid Mech. 72 (1975) 391, https://doi.org/10.1017/s0022112075003448.
[22] J.D. Jackson, Classical electrodynamics, Wiley, New York, 1962 https://doi.org/10.13140/RG.2.2.29746.09928.
[23] J.R. Blake, D.C. Gibson, Cavitation bubbles near boundaries, Annu. Rev. Fluid Mech. 19 (1987) 99–123, https://doi.org/10.1146/annurev.fl.19.010187.000531.
[24] X. Huang, H. Hu, S. Li, A. Zhang, Nonlinear dynamics of a cavitation bubble pair near a rigid boundary in a standing ultrasonic wave field, Ultrason. Sonochem. 64 (2020), 104969, https://doi.org/10.1016/j.ultsonch.2020.104969.
[25] H. Wu, H. Zheng, Y. Li, C.D. Ohl, H. Yu, D. Li, Effects of surface tension on the dynamics of a single micro bubble near a rigid wall in an ultrasonic field, Ultrason. Sonochem. 78 (2021), 105735, https://doi.org/10.1016/j.ultsonch.2021.105735.
[26] X. Wang, W. Chen, M. Zhou, Z. Zhang, L. Zhang, Influence of rigid wall on the nonlinear pulsation of nearby bubble, Ultrason. Sonochem. 87 (2022), 106034, https://doi.org/10.1016/j.ultsonch.2022.106034.